Unsteady Model Estimation for Generic T-Tail Transport Aircraft Using Computational Data

Patrick C. Murphy,[1] Neal Frink,[2] S. Naomi McMillin,[3] Kevin Cunningham,[4] and Gautam H. Shah[5]
NASA Langley Research Center, Hampton, VA 23681

Models including nonlinear and unsteady behaviors are developed for the longitudinal axis of the NASA Generic T-Tail Aircraft over a large range of angle of attack. These models are based on computational simulations of forced-oscillation tests in a wind tunnel. This work continues a recent study and an ongoing effort by NASA to improve aircraft simulations for pilot training in loss-of-control and stalled conditions. The objective of this work is to develop appropriate aerodynamic models that provide representative responses in simulation for a given class of aircraft. In the stall region, nonlinear unsteady responses are often present and may require an extended aerodynamic model compared to that used in the conventional flight envelope. In this study, two objectives are addressed. The first is to obtain representative models for the NASA Generic T-Tail aircraft over a wide range of angle of attack and the second is to continue development of a specialized CFD test technique that uses Schroeder sweeps to create information rich responses for unsteady aerodynamic model identification.

I. Nomenclature

A_j, B_j	=	Fourier coefficients
a, b_1	=	deficiency function parameters
b	=	wing span, ft
C_N	=	normal force coefficient
C_m	=	pitching-moment coefficients
$\bar{c}$	=	mean aerodynamic chord, ft
F_{a_α}	=	deficiency function
f	=	frequency, Hz
k	=	reduced f, $\pi \bar{c} f / V$
m	=	no. of harmonics in Fourier expansion
N	=	number of data points
q	=	pitch rate, rad/sec
R^2	=	coefficient of determination
S	=	reference area, ft^2
t	=	time, s
V	=	velocity, fps
α	=	angle-of-attack, rad or deg
α_0	=	initial angle-of-attack in forced oscillation experiments, rad or deg
δC_m	=	change in value of C_m from C_{m0}
η	=	state variable
σ	=	standard error
τ	=	dummy integration variable
τ_1	=	non-dimensional time constant, $\frac{1}{b_1}\left(\frac{2V}{\bar{c}}\right)$
ω	=	angular frequency, rad/sec
$\bar{C}_{a_\alpha}$	=	in-phase coefficient
$\bar{C}_{a_q}$	=	out-of-phase coefficient
SS_E, SS_r	=	residual and total sum of squares

Subscripts

A	=	amplitude
a	=	aero forces and moments: N *or* m
E	=	measured value

Superscripts

^	=	estimated value
~	=	mean value

[1] Senior Research Engineer, Dynamic Systems and Control Branch, MS 308, Associate Fellow.
[2] Senior Research Engineer, Configuration Aerodynamics Branch, MS 499, Associate Fellow.
[3] Research Aerospace Engineer, Configuration Aerodynamics Branch, MS 499, Member.
[4] Senior Research Engineer, Flight Dynamic Branch, MS 308, Senior Member.
[5] Senior Research Engineer, Flight Dynamic Branch, MS 308, Associate Fellow.

II. Introduction

The NASA Technologies for Airplane State Awareness (TASA), a sub-project of the NASA Airspace Operations and Safety Program, is completing research on developing representative models for various classes of transport aircraft. In this study, efforts were focused on models appropriate for the NASA Generic T-Tail (GTT), aft twin-engine, configuration [1-2], shown in Fig.1. One goal of the current study is to develop high-fidelity aerodynamic models over a large flight envelope, including the stall region, which can be used in training simulations. Modeling for GTT has been applied to piloted simulations in [3]. In addition, modeling techniques continue to be developed that facilitate efficient testing and estimation of high-fidelity mathematical models. These models are developed using aircraft System Identification (SID) and Computational Fluid Dynamics (CFD) tools. SID tools are applied to CFD simulated measurements of the GTT during simulated forced-oscillation tests to obtain unsteady models that allow prediction of nonlinear unsteady behaviors and that are suitable for flight dynamics studies.

Efficient inputs for unsteady modeling have been well established for wind-tunnel forced-oscillation tests. Early studies [4] demonstrated the best practices in using sinusoids, ramps, and wide-band inputs. Single-frequency sinusoidal inputs provide diagnostic information as well as facilitate estimation of unsteady models. Wide-band inputs provide a more efficient data source for estimation and ramp-and-hold inputs offer useful validation data. This discussion is also considered in later reports [5-6] that provide a broader discussion of unsteady modeling. Since CFD can be computationally demanding, the current study continues a recent investigation in [7] that considered these three inputs applied to the GTT model in CFD simulation of forced-oscillation tests. The initial investigation in [7] found that single-frequency forced-oscillation inputs were the preferred method. Step inputs, as applied in [7], were found to be susceptible to noise and other harmonics or nonlinearities that may be present. Wide-band inputs, in the form of Schroeder sweeps, were found to be too computationally demanding in terms of total computational time (excluding wait time in queues) or "wall-clock" time. The Schroeder sweep has proven to be very effective in wind-tunnel dynamic tests since it provides a flat power spectrum over the frequency range of interest. Consequently, investigation is continued in this study to add some guidance for CFD applied to wide-band inputs. In this study a number of CFD modeling parameters were changed from those used in [7] to reduce processing time for the wide-band input.

In this study, two objectives are addressed. The first objective is to obtain representative models for the NASA Generic T-Tail aircraft (GTT), over a wide range angle of attack using sinusoidal inputs in pitch forced-oscillations. The previous study [7] was limited to one angle of attack to allow a focused study where nonlinear and unsteady effects were maximized. Details of CFD simulated responses are described in [8-9]. The second objective is to evaluate the specialized CFD test technique using Schroeder sweeps. The later results contribute toward understanding the best practices for estimating unsteady models using CFD simulated experiments.

III. Computational Data

CFD predictions were performed with the USM3D flow solver [10] that is part of the NASA Tetrahedral Unstructured Software System (TetrUSS) [11]. USM3D is a parallelized tetrahedral cell-centered, finite volume compressible Reynolds-averaged Navier-Stokes (RANS) flow solver. The term "cell centered" means that the finite volume flow solution is solved at the centroid of each tetrahedral cell. Inviscid flux quantities are computed across each tetrahedral cell face using various upwind schemes. Spatial discretization is accomplished by a novel reconstruction process, based on an analytical formulation for computing solution gradients within tetrahedral cells. The solution can be advanced in time by a second order "physical" time step scheme, a second order "dual" time step scheme, or to a steady-state condition by an implicit backward-Euler scheme. Several turbulence models are available including the one-equation Spalart-Allmaras (SA) model and several two-equation models. The two-equation models available are the Jones and Launder k-ε model, Menter Shear Stress Transport (SST) model, nonlinear Algebraic Reynolds Stress Models (ARSM) of Girimaji and Shih/Zhu/Lumley, and the Wilcox 1988 k-ω model. Detached Eddy Simulation (DES) has been implemented in all of the turbulence models. A capability to trip the flow at specified locations on aerodynamic surfaces has been implemented for the k-ε turbulence model, but fully turbulent flow was assumed for the results in this paper. USM3D has capabilities for overset grids and dynamic grid motion, the latter being used in the current study. Published guidelines [12] for computing dynamic forced oscillation solutions were employed for the CFD computations in this study. CFD simulations were generated that correspond to the pitch forced-oscillation wind tunnel tests performed on the GTT in the regions of interest.

IV. Experimental Data

Expanding on the study in [7], the new data in this study come from CFD simulated forced-oscillations of the GTT model. These data allow aerodynamic models of C_N and C_m, with the appropriate level of complexity, to be estimated over the range of angle of attack. Table 1 shows the range of angle of attack and frequencies considered. The CFD

responses were computed to simulate equivalent sinusoidal, pitch-axis, forced-oscillations in the LaRC 12-Foot Low Speed Wind Tunnel with 5° amplitude. Two sets of data were considered, labeled as 1st and 2nd in Table 1. Harmonic analysis was used to obtain conventional in-phase and out-of-phase damping coefficients for frequency cases labeled 1st. This determined the angle of attack cases where frequency-dependent behavior occurred and requires unsteady modeling. This approach prevented unnecessary computations at additional forced-oscillation frequencies in regions where unsteady behaviors were not present. In the first set, frequency effects were explored over a range of angle of attack, from 0° to 40°, for the initial screening and diagnosis. Only three frequencies, representing a relatively large range from high to low, were needed to determine if sufficient spread in the frequency response is present. Once located, additional frequencies were added to allow estimation of the unsteady model transfer function. For the second set, the effects of seven different non-dimensional frequencies from 0.0079 to 0.040 were investigated over the range of angle of attack where unsteady behavior was indicated.

Table 1. Test cases for longitudinal models.

Non-dimensional Frequency	0.0079	0.012	0.0158	0.020	0.025	0.0316	0.040
Angle of Attack (degrees)							
4	1st			1st			1st
8	1st			1st			1st
10	1st	2nd	2nd	1st	2nd	2nd	1st
12	1st	2nd	2nd	1st	2nd	2nd	1st
14	1st	2nd	2nd	1st	2nd	2nd	1st
16	1st	2nd	2nd	1st	2nd	2nd	1st
18	1st	2nd	2nd	1st	2nd	2nd	1st
20	1st	2nd	2nd	1st	2nd	2nd	1st
22	1st	2nd	2nd	1st	2nd	2nd	1st
24	1st			1st			1st
28	1st			1st			1st
30	1st			1st			1st
35	1st			1st			1st
40	1st			1st			1st

V. Aerodynamic Modeling

Identifying an adequate aerodynamic model requires a clear definition of the requirements and intended use for that model, as well as an appropriately designed test to allow identification. A general model and recommended test techniques developed for nonlinear unsteady conditions has been developed over a number of years and is summarized in Ref. [5]. The current study extends the analysis in [7] to a larger range of angle of attack and only considers responses in the longitudinal axis. Limited results in the lateral axis from [7] are included to explain the choice of input types made in this study. The following section presents model structures applied in the longitudinal axis for this study, however, the corresponding discussion for the lateral axis can be found in [7].

A. General Unsteady Model

Aerodynamic coefficients, C_N and C_m, are represented by C_a, where subscript *a* represents *N or m.* Model structures for the aerodynamic coefficients utilized in this study are given below. In this study, a linear unsteady model structure was used and found to be adequate. Under limited motion assumptions [5], this model structure allows estimated parameters to vary with α, thus allowing a broad class of nonlinear aerodynamic responses to be captured. Each longitudinal coefficients can be written as

$$C_a(t) = C_a(0) + \int_0^t C_{a_\alpha}(t-\tau)\dot{\alpha}(\tau)d\tau + \frac{\bar{c}}{2V}\int_0^t C_{a_q}(t-\tau)\dot{q}(\tau)d\tau \tag{1}$$

In Eq. (1) coefficients $C_{a_\alpha}(t)$, and $C_{a_q}(t)$, are the indicial functions and $C_a(0)$ is the initial value of C_a. Two assumptions [13] are adopted to simplify the model: (a) the effect of angular acceleration $\dot{q}$ on any coefficient can be neglected and (b) the indicial functions in Eq. (1) can be expressed as

$$C_{a_\alpha}(t) = C_{a_\alpha}(\infty) - F_{a_\alpha}(t) \tag{2}$$

where $F_{a_\alpha}(t)$ is the deficiency functions and $C_{a_\alpha}(\infty)$ is the rate of change C_a with α evaluated in steady flow conditions.

The simplified model, which takes into account changes with respect to steady state, has the form

$$C_a(t) = C_{a_\alpha}(\infty)\alpha(t) + \frac{\bar{c}}{2V} C_{a_q}(\infty) q(t) - \int_0^t F_{a_\alpha}(t-\tau)\dot{\alpha}(\tau) d\tau \tag{3}$$

To obtain a model appropriate for identification and with a limited number of parameters, the deficiency function is assumed to be a simple exponential function

$$F_{a_\alpha} = a e^{-b_1 t} \tag{4}$$

Models appropriate for an aircraft undergoing one degree-of-freedom forced oscillation in pitch can be obtained using Eqs. (3) and (4). Considering one degree-of-freedom pitching motion in the tunnel

$$C_a(t) = C_a[\theta(t), q(t)] \tag{5}$$

where pitch and angle-of-attack are constrained by the physical test arrangement and thus related by the equality (for upright oscillations)

$$\alpha(t) = \theta(t) \tag{6}$$

Combining Eqs. (3-6), the aerodynamic models can be formulated as

$$C_a(t) = C_{a_\alpha}(\infty)\alpha(t) + \frac{\bar{c}}{2V} C_{a_q}(\infty) q(t) - a\int_0^t e^{-b_1(t-\tau)}\dot{\alpha}(\tau) d\tau \tag{7}$$

By introducing

$$\eta(t) = \int_0^t e^{-b_1(t-\tau)}\dot{\alpha}(\tau) d\tau \tag{8}$$

and applying the Leibniz integral rule, the state space form of Eq. (7) can be written as

$$\dot{\eta}(t) = -b_1\eta(t) + \dot{\alpha}(t) \tag{9}$$

$$C_a(t) = C_{a_\alpha}(\infty)\alpha(t) + \frac{\bar{c}}{2V} C_{a_q}(\infty) q(t) - a\eta(t) \tag{10}$$

From Eq. (7), a steady response can be written as

$$C_a(t) = \bar{C}_{a_\alpha}\alpha_A \sin(\omega t) + \bar{C}_{a_q}\alpha_A k \cos(\omega t) \tag{11}$$

where α_A is the amplitude of pitch oscillation, k is reduced frequency, and $\bar{C}_{a_\alpha}$ and $\bar{C}_{a_q}$ are the in-phase and out-of-phase components, respectively. These components are related to the model parameters (aerodynamic derivatives) by the equations

$$\bar{C}_{a_\alpha} = C_{a_\alpha}(\infty) - a\frac{\tau_1^2 k^2}{1+\tau_1^2 k^2} \tag{12}$$

$$\bar{C}_{a_q} = C_{a_q}(\infty) - a\frac{\tau_1}{1+\tau_1^2 k^2} \tag{13}$$

B. Experiment Design Considerations

Aircraft SID provides a large body of knowledge on best practices for identifying aerodynamic models from flight or ground-based experimental facilities. Aircraft SID methods, in general, are described in [14] and SID methods focused on estimating unsteady models in a ground-based environment are described in [5]. Practitioners know that a well-designed experiment is required to achieve useful and validated mathematical models. For example, forced-oscillation frequencies chosen based on short-period mode frequencies will provide useful damping data but will likely miss any rigid-body unsteady behaviors. As indicated by Eqs. (12, 13), as the forced-oscillation frequencies become larger the unsteady term is diminished relative to the steady-flow damping term.

In general, careful input design with a wide range of amplitudes and frequencies will provide sufficient information content for complete model identification. Fig. 2 shows a flow chart of the SID process with large blue arrows added to highlight where the standard process is modified for unsteady modeling. At the bottom of the figure the concept of Harmonic Analysis is highlighted. This is a diagnostic tool, used in combination with single-frequency forced-oscillation tests, that allows detection of unsteady behaviors and identifies the angle of attack and frequency ranges where it may occur. In addition, this analysis provides some guidance on the degree of nonlinear behaviors that might be present. With this guidance, the appropriate model structures and parameter estimation methods can be selected. Also shown in Fig. 2 is a list of specialized inputs that work well for this type of modeling. Different parameter estimation methods may be applicable depending on how the unsteady behaviors manifest. A two-step regression is useful when unsteady behavior presents in both in-phase and out-of-phase components of the response, however, the aerodynamic model is assumed to be linear for that option. If the unsteady behavior is only present in the out-of-phase component, then nonlinear regression is utilized. Equation error and output error are generally applied to linear and nonlinear aerodynamic cases, respectively.

Fig. 3 shows examples of useful inputs for identification and validation of unsteady models and applicable to any axis. These types of inputs require a test facility that allows programmable motions. In general ground-based experimental testing, sinusoidal inputs are suited for harmonic analysis, wide-band inputs for efficient modeling, and ramps for model validation data. A key characteristic of the two wide-band inputs is the enforcement of a flat power spectrum. This ensures that enough excitation is provided evenly over the specified frequency band.

C. Harmonic Analysis

Harmonic analysis provides a key diagnostic tool. It allows detection of unsteady behaviors and defines the range of frequencies and angles of attack where unsteady behavior occurs. In addition, it gives some guidance on the degree of nonlinearities when present. A conventional aerodynamic model assumed in forced-oscillation testing is given by Eq. (11). The form used for harmonic analysis can be written as

$$C_a(t) = A_0 + \sum_{j=1}^{m} A_j \cos(j\omega t) + \sum_{j=1}^{m} B_j \sin(j\omega t) \tag{14}$$

The unknown parameters, A_0, A_j, and B_j, are the Fourier series coefficients that are directly related to the in-phase and out-of-phase coefficients normally obtained in forced-oscillation experiments. Harmonic analysis provides estimates of these coefficients, their standard errors, and the Coefficient of Determination, R^2. Since the terms in this series are orthogonal, they do not change value when additional higher-order terms are added. Higher-order terms are necessary when the aerodynamic response is nonlinear. If the first-order harmonic case (j = 1) terms provide an adequate fit to the data then only a linear aerodynamic model is required. If, in addition, no frequency dependence is

present, then only a conventional damping term is required in the model. This can be seen by considering Eq. (10), where three distinctly different terms model the static, steady-flow dynamic, and unsteady responses.

For the model with linear aerodynamics and A_0 = 0, the aerodynamic in-phase and out-of-phase components can be expressed in terms of the coefficients A_1 and B_1. For pitch oscillation the expressions are

$$\bar{C}_{a_\alpha} = \frac{B_1}{\alpha_A} \tag{15}$$

$$\bar{C}_{a_q} = \frac{A_1}{k\alpha_A} \tag{16}$$

Another key part of harmonic analysis that helps sort details about the required model structure is the use of the Coefficient of Determination, R^2. This statistical metric indicates the fraction of the variation in measured data explained by the model and is defined as

$$R^2 = 1 - SS_E / \mathrm{SS}_r \qquad 0 < R^2 < 1 \tag{17}$$

where

$$SS_E = \sum_{i=1}^{N} [C_{a_E}(i) - \hat{C}_a(i)]^2 \tag{18}$$

is the residual sum of squares and

$$SS_r = \sum_{i=1}^{N} [C_{a_E}(i) - \tilde{C}_a(i)]^2 \tag{19}$$

is the total sum of squares. $C_{a_E}(i), \hat{C}_a(i),$ and $\tilde{C}_a(i)$ are the measured, estimated, and mean values, respectively.

D. Parameter Estimation Method

Parameter estimation for this study will use a variation of an output-error method [5] in the time domain. Output error in the time domain is a more general method that allows estimation of a full unsteady model that may have linear or nonlinear terms in the model. In this study, the model equations given by the state-space equations, noted in Eqs. (9-10), were applied to the longitudinal axis. Measured time histories of inputs, α, and outputs, C_a, for each of the frequencies tested, are combined or "stacked" to ensure all the frequency content is included in the time domain estimation process. Equation integrations must be performed separately for each frequency forced-oscillation test but a single cost function is used to capture the overall model effectiveness. Application of the general output-error method for aircraft is explained in [14] and relevant software is provided in [15].

VI. Results and Discussion

Supporting the current investigation are key results from [7] that highlighted the preferred use of single-frequency sinusoids and wide-band inputs for estimating nonlinear unsteady models. Fig. 4 presents the estimation errors that confirmed this conclusion. Results from the previous study, shown in Fig. 4, are based on a simulation of an unmanned aircraft where the aerodynamic model was known exactly. The three different types of inputs demonstrate the quality of those inputs in providing information content for system identification. The three inputs were composed of six sinusoids, four ramps at different rates, and one Schroeder sweep designed for the same range of frequencies all applied to the roll axis. The results highlight that, in a benign (relatively low noise) test, the ramp inputs were significantly less effective. In addition, initial pitch-axis tests presented in [7] using CFD 50-second Schroeder sweeps were abandoned due to the overly burdensome wall-clock time (order of weeks) for computation. Investigations in this study continue with CFD simulated sinusoidal pitch-axis forced-oscillations, however, parameter settings in the CFD tools are adjusted to speed up simulation of the wide-band input.

A. Harmonic Analysis

With application of Eq. (14) for harmonic analysis and Eq. (17) to test linear model fit, both provide an initial diagnostic tool that readily identifies where unsteady behaviors occur and where either noise or nonlinearities are dominating the response. If the in-phase and out-of-phase components estimated in Eq. (14) show frequency dependence then unsteady behavior is indicated. Where values of R^2 for the first-order harmonics are high (experience dictates that values of $R^2 \geq 0.8$ are high in a wind-tunnel environment) then a linear model structure is indicated. Lower values of R^2 usually indicate a need for further investigation. The investigation needs to determine whether higher harmonics are required due to nonlinearities or simply the presence of relatively high noise.

Estimates of R^2 are influenced by the value and number of Fourier coefficients (harmonic order) in Eq. (14) and the measurement noise. However, R^2 is an effective diagnostic tool to determine adequacy of a linear first-order model against nonlinear higher harmonic models because the harmonic sinusoids are mutually orthogonal. The estimates of A_j and B_j will not change with the number of model terms included. Changes will only appear in the corresponding standard errors and residuals defined by Eq. (17).

1. Harmonic Analysis for GTT model, CFD Simulated Test Case 1

Harmonic analysis over the full range of angle of attack, defined in Table 1 as the 1st test case with three frequencies, reveals the unsteady aerodynamic behaviors for the GTT aircraft. The three frequencies were chosen to ensure any unsteady behavior would be unmasked. Based on results in [7], the highest, lowest, and middle frequencies were chosen for this screening process. Figure 5a presents C_N in-phase and out-of-phase coefficients for first-order harmonic analysis. High values for R^2 indicate linear models are adequate within the 5° amplitude motion and over the full α range. No frequency dependence occurs in the in-phase coefficient and limited dependence occurs in the out-of-phase coefficient specifically at α = [8, 12, 14, 18] degrees. At many angles of attack the out-of-phase coefficients do not vary with frequency. The lack of frequency spread indicates little, if any, unsteady behavior and consequently any attempt to identify an unsteady model will fail.

Figure 5b presents a first-order harmonic analysis for C_m in-phase and out-of-phase coefficients. Similar to the normal force results virtually no frequency dependence is present for the in-phase coefficient. For the out-of-phase coefficient well-defined frequency spreads or dependence occurs at α = [12, 14, 16, 35, 40] degrees. Given project interest in $\alpha > 10°$ cases for simulation and these current results, additional frequencies were added to allow study of C_m in the range of $10° < \alpha < 22°$.

2. Harmonic Analysis for GTT model, CFD Simulated Test Case 2

Harmonic analysis over a reduced range of angle of attack ($10° < \alpha < 22°$), defined in Table 1 as the 2nd test case with seven frequencies, provides more resolution of the frequency spreads and additional frequency content to allow unsteady model estimation.

Figure 6a presents C_N in-phase and out-of-phase coefficients for first-order harmonic analysis using seven frequencies. Confirming results from Fig. 5a, high values for R^2 indicate linear models are adequate within the 5° amplitude motion. No frequency dependence occurs in the in-phase coefficient and very limited dependence occurs in the out-of-phase coefficient specifically at α = [12, 14, 18] degrees.

Figure 6b presents first-order harmonic analysis for C_m in-phase and out-of-phase coefficients. Confirming results in Fig. 5b, virtually no frequency dependence is present for the in-phase coefficient. For the out-of-phase coefficient, well-defined frequency spreads only occur at α = [12, 14, 16] degrees. As was noted in [7] and shown in Fig. 5b, the lowest R^2 occurs at 16° angle of attack.

In the previous study [7], up to a third-order harmonic analysis at α = 16 degrees, was required to obtain adequate R^2 values greater than 0.8 (or 80%). Results of that analysis for the frequencies of interest are presented here in Table 2 and Table 3. Table 2 reveals that normal force is well modeled using a linear unsteady model. However, the pitching moment case is notably different with none of the values above 80%. Table 3 shows the third-order harmonic models fit the responses reasonably well based on R^2 values. The need for higher harmonics indicates that some nonlinearities or very poor signal-to-noise may be present.

As an example, the first and third-order harmonic model fits are shown in Fig. 7 for the worst-case R^2 that occurred at the lowest frequency. The CFD simulated data is presented in the figure as blue "+" symbols and labeled "mean cycle data" which is the average of all the cycles analyzed. The green line shows the first-order harmonic model and red line shows the third-order model. The significantly better fit of the third-order harmonic model demonstrates the improved fit achieved with a cubic nonlinearity. The graphics also demonstrate the significant changes in responses between linear and higher-order polynomial terms in the aerodynamic models. The mean cycle data reveals the higher harmonics present in the CFD simulated forced-oscillation data. Depending on the modeling application, engineering

judgement is required to determine whether it is necessary to model these higher harmonics. For purposes of this study, the primary goal is to identify representative models that capture the primary responses. In this case, capturing the cubic nonlinearity and unsteady behaviors are sufficient. In general, if more complexity is required in any of the three terms in Eq. (10) then choosing smaller amplitude oscillations is an option that will drive the models closer to linear response. Alternative model structures are also an option for more complex dynamics, such as described in [16]. Avoiding high-order polynomials is desirable to limit the number of unknown parameters to a size that matches the information content of the dynamic response data.

Table 2. First-order harmonic model adequacy at α = 16°, based on R^2.

	1	2	3	4	5	6	7
k	0.0079	0.0120	0.0158	0.0200	0.0250	0.0316	0.0400
R^2 for *CN (%)*	88.5	86.0	93.7	94.4	94.8	97.5	98.4
R^2 for *Cm (%)*	20.2	28.3	35.3	44.6	55.9	64.6	77.2

Table 3. Third-order harmonic model adequacy at α = 16° based on R^2.

	1	2	3	4	5	6	7
k	0.0079	0.0120	0.0158	0.0200	0.0250	0.0316	0.0400
R^2 for *CN*	97.3	94.5	98.6	99.5	99.1	99.3	99.7
R^2 for *Cm*	83.4	86.5	90.4	97.5	96.8	97.1	98.6

B. Unsteady Model Identification

Two modeling problems are addressed in this section: (1) using CFD to simulate forced-oscillation tests of the GTT to allow unsteady model estimation and (2) using SID to identify unsteady models from the CFD simulated data. In the first case, the challenge was to provide data over a large range of angle of attack and frequencies of oscillation. In addition, an effort continues toward developing guidance on the best CFD settings when modeling the responses to Schroeder sweeps. In the second case, the challenge was to identify representative aerodynamic models for the GTT configuration that capture damping and unsteady responses as required.

1. CFD Simulated Test Data for GTT

The forced-oscillation CFD solutions were computed using USM3D with Spalart-Allmaras turbulence model on a half-span GTT grid of 28.8 million tetrahedral cells. Since USM3D is formulated as a compressible RANS flow solver, numerical convergence and accuracy degrades rapidly for very low Mach numbers. Since the 12FT wind tunnel data was measured at M_∞=0.052, a higher M_∞=0.126 was prescribed for the USM3D solutions to insure good numerical convergence. Furthermore, the CFD geometry is based on the larger subscale flying model with $\bar{c}$ =21.204 inches whereas the wind-tunnel model has a $\bar{c}$ =7.7612 inches. Hence, it was necessary to scale the CFD motion time scale to match the reduced frequencies of the wind-tunnel data. Since reduced frequency is simply the ratio of a velocity at the end of a rotating reference length relative to the oncoming velocity, the scaled CFD frequency is defined in Eq. (20). Once a solution is complete, then the time is rescaled back to the wind-tunnel conditions.

$$f_{CFD} = f_{WT}(\bar{c} / M_\infty)_{WT}(M_\infty / \bar{c})_{CFD} \tag{20}$$

The pitch forced oscillation (FO) cases were run for two full cycles with 1800-time steps per cycle, for a total of 3600-time steps. Each time step was converged with 40 subiterations. The final number of time steps is noted in Table 4.

As discussed in Ref. [7], computing a Schroeder sweep of 50-second duration with the all-tetrahedral 28.8 million cell grid was estimated to require weeks of run time and was thus not attempted. For the present study, a new developmental mix-element version of USM3D [17] was utilized and a new grid comprised of a mix of 8.7 million prism and tetrahedral elements was generated.

The objectives for using CFD simulated data were to obtain unsteady models to help corroborate or gain insights into the experimental results and to evaluate test and modeling techniques. Besides accuracy, one aspect of technique evaluation is to consider the efficiency or resources required to obtain data. Two metrics to consider are the Central Processing Unit (CPU) usage and the wall-clock time of the computations. Simulations were run until sinusoids reached steady-harmonic oscillations. A 50-second Schroeder sweep was considered only for the nominal 16° angle of attack condition. The sinusoidal forced oscillation calculations are all performed on the NASA Langley Research

Center K3 machine using 144 processors. The 50-second Schroeder sweep was computed on the NASA Advanced Supercomputing (NAS) facility's Pleiades supercomputer Ivy Bridge nodes. Table 4 shows the CPU time required for each input type. The sinusoidal solutions required approximately 1 week of run time to compute six frequencies. The Schroeder sweep required approximately 4 days to compute a wide-band input at one angle of attack.

Table 4a. CFD Computational Requirements for GTT 2-cycle Sinusoids, α_0=16°, α_A=5°, 28.8M cells.

	K3 CPU hours	K3 wall-clock time, 144 processors
Initial Static	1104	7.7 hours
Single-frequency, 3600 time steps	8350	2.4 days
Six-frequency	50100	~ 1 week (cases run in parallel)

Table 4b. CFD Computational Requirements for GTT Schroeder sweep, α_0=16°, α_A=5°, 8.7M cells.

	No. time steps	Δt*	Pleiades CPU hours	Pleiades wall-clock time, 192 processors
Initial Static	6000	0.1	2200	11.5 hours
Schroeder	76000	0.06	16630	3.6 days

2. Model Identification Using CFD Simulated Test Data for GTT

Based on harmonic analysis results, shown in Tables 2-3, the more challenging modeling problem is presented in the pitching moment data. In addition, Fig. 7 presented a clear indication that C_m will likely require nonlinear-unsteady models in the stall region. The lowest frequency case, in Fig. 7, also demonstrated that some of the responses included higher-order dynamics not of interest to this study. To make this paper more tractable, the remaining discussion will focus on modeling the C_m response.

Results of the unsteady model analysis for GTT, at α = 16°, are given in Table 5. Trim settings are removed from the data so C_{m0} reflects a residual bias term not the nominal aerodynamic moment. CFD forced-oscillation data was restricted to six frequencies to represent a typical minimum set of data available for modeling and to allow the seventh frequency case for a validation test. In this case the middle frequency is reserved for validation testing. Table 5a provides the estimated static model for each input type. Table 5b provides the corresponding unsteady model. In order to get an adequate model, the static model required a cubic polynomial, as expected based on harmonic analysis of the sinusoidal responses.

Table 5a. Estimated Static Model from CFD Simulation of GTT at α_0 = 16 deg.

Parameter	Input type	C_{m_0}	C_{m_α}	$C_{m_{\alpha^2}}$	$C_{m_{\alpha^3}}$
Estimate, $\hat{\theta}$ ($\hat{\sigma}$)	sinusoids	0.0290 (0.0007)	1.2840 (0.0329)	-7.5678 (0.1492)	-164.7890 (3.4225)
Estimate, $\hat{\theta}$ ($\hat{\sigma}$)	Schroeder sweep	0.0155 (0.0004)	1.0724 (0.0139)	-7.5270 (0.1570)	-164.3931 (4.2306)

Table 5b. Estimated Unsteady Model from CFD Simulation of GTT at α_0 = 16 deg.

Parameter	Input type	C_{m_q}	$C_{m_{q\alpha}}$	a	b_1	τ_1	R^2
Estimate, $\hat{\theta}$ ($\hat{\sigma}$)	sinusoids	-25.5142 (0.4877)	467.7928 (7.8594)	0.3705 (0.0211)	1.4982 (0.1726)	121.9115 (14.0448)	0.75
Estimate, $\hat{\theta}$ ($\hat{\sigma}$)	Schroeder sweep	-27.7817 (0.2010)	354.1475 (6.2469)	0.3705 (fixed)	1.49.82 (fixed)	121.9115 (fixed)	0.97

The Schroeder sweep data allowed estimation of a comparable model but the results are limited. Currently the authors believe that the aggressive reduction in grid size, to allow faster computations, limited the information content and prevented estimation of the unsteady terms. Consequently, estimation of the remaining model terms required the unsteady terms be held constant or "fixed" during parameter estimation. The resulting models and model predictions are very good and match sinusoidal results very well. Results are shown in Table 5 and model prediction compared to simulated measurements in Fig. 8.

Figures 9-10 show the measured and predicted responses for a third-order model based on the sinusoidal CFD data. The two figures show the low and high frequency case. Both predicted (red line) and measured responses (green "+") are shown as changes from the nominal oscillation condition at α_0 = 16 degrees. Included in the figures are blue lines, representing the estimated static model. The model provides an adequate representation of the dynamics provided by CFD simulation given the objective of obtaining a representative model. In this complex aerodynamic region at α = 16° the rapidly changing statics and dynamics are better predicted by a more general model.

A validation test of the unsteady model from sinusoidal data is shown in Fig. 11. In this case, the final model is used to predict responses for the middle frequency case (k = 0.020). For this portion of the study, the middle frequency was not included in the data for estimation. The results show the model is adequate as a representative model that captures the dominate features of the response indicated by CFD simulation. The validation test produced an R^2 value of 80.1%.

Unsteady responses of interest for C_m occur at α_0 = [12, 14, 16] degrees. Using CFD sinusoidal data, models identified for those cases are given in Table 6. For these models all seven frequencies were included in the data.

Table 6a. Estimated Static Model from CFD Simulation of GTT.

Parameter	α_0	C_{m_0}	C_{m_α}	$C_{m_{\alpha^2}}$	$C_{m_{\alpha^3}}$
Estimate, $\hat{\theta}$ ($\hat{\sigma}$)	12	-0.0399 (0.0005)	0.2827 (0.0187)	10.5311 (0.1147)	43.2240 (2.6317)
Estimate, $\hat{\theta}$ ($\hat{\sigma}$)	14	-0.0156 (0.0007)	1.2473 (0.0253)	4.1395 (0.1483)	-103.7732 (3.4014)
Estimate, $\hat{\theta}$ ($\hat{\sigma}$)	16	0.0266 (0.0006)	1.3110 (0.0293)	-6.9449 (0.1388)	-172.4126 (3.1838)

Table 6b. Estimated Unsteady Model from CFD Simulation of GTT.

Parameter	α_0	C_{m_q}	$C_{m_{q\alpha}}$	a	b_1	τ_1	R^2
Estimate, $\hat{\theta}$ ($\hat{\sigma}$)	12	-49.8981 (0.5345)	13.9824 (6.0060)	0.4803 (0.0208)	3.0847 (0.2072)	59.2106 (3.9772)	0.91
Estimate, $\hat{\theta}$ ($\hat{\sigma}$)	14	-42.1554 (0.6253)	443.2878 (7.7624)	0.4497 (0.0220)	2.6013 (0.2288)	70.2134 (6.1756)	0.83
Estimate, $\hat{\theta}$ ($\hat{\sigma}$)	16	-25.6645 (0.4847)	486.3530 (7.2659)	0.3747 (0.0191)	1.6522 (0.1720)	110.5469 (11.5083)	0.76

Figure 12 shows the basic trends of the aerodynamic models for the pitching moment without plotting all the polynomial terms. The variation of three major terms in the models, ($C_{m_{q0}}$, a, τ_1), at the nominal α_0 conditions, are presented in the figure over the full range of angle of attack considered in this study. Since parameters for the unsteady model τ_1 and a are the non-dimensional time constant and gain for the unsteady transfer function, each must reduce to zero in locations without an unsteady term. The damping terms were estimated as linear polynomials but only the first term is plotted in Fig. 12. Unsteady terms were not computed at the highest angles of attack (35° and 40°), although harmonic analysis indicated unsteady terms were present. Responses for only three frequencies were computed consequently unsteady models could not be estimated. This range of angle of attack was outside the primary region of interest in this study.

VII. Concluding Remarks

Model identification work in this study completed a previous effort where evaluation of tools and techniques for unsteady model identification and estimation of representative longitudinal aerodynamic models for the NASA GTT aircraft was initiated. These two studies promoted development and application of CFD to stability and control problems. CFD was applied to simulate wind-tunnel forced-oscillation testing over a wide range of angle of attack for the GTT aircraft.

The previous study was limited to 16° angle of attack in order to ensure a point in the GTT flight envelope was chosen with distinctly nonlinear and unsteady behaviors. This test point provided challenging tests for the methodologies involved. In the current study a larger range of angle of attack, from 4° to 40°, was investigated allowing assessment of the appropriate model complexity for the GTT configuration, longitudinal dynamics, based on CFD simulated oscillatory data.

The previous study focused on using three different, commonly used inputs, for experimental testing: (1) sinusoidal forced-oscillation, (2) ramp-and-hold, and (3) a wide-band sweep. Initial screening using simulated data demonstrated the more effective inputs were sinusoidal and wide-band sweeps. The advantages of application of single-frequency sinusoids, as a diagnostic tool, to dynamic systems was demonstrated in both the current and previous study. The location and severity of nonlinearities were determined using harmonic analysis of the sinusoidal data. Both of the more effective inputs ensured frequency content over the range of interest and the wide-band input (Schroeder sweep) provided a flat power spectrum. All three inputs have been applied to the NASA GTT model in CFD simulation but the wide-band input was eliminated in the previous study due to an unacceptable computational time. In the current study, evaluation and development of the specialized CFD wide-band test input continued in an effort to reduce the computational expense. After substantial reduction in grid size, the Schroeder sweep data allowed estimation of a comparable model but the results were limited and excluded estimation of the unsteady terms. Currently the authors believe that the aggressive reduction in grid size limited the information content and prevented estimation of the unsteady terms.

A primary objective for this study was to find representative models for the GTT class of vehicle, not specific, high-fidelity, models for a given experimental vehicle. As is often the case, a subject matter expert or simulation engineer using the models would need to provide guidance as to the level of complexity that makes sense for their application. For the current model structure, going beyond cubic expansions for each parameter may lead to a requirement for more data with proper information content to sufficiently characterize that more complex model.

Acknowledgments

The authors extend their appreciation to the Vehicle Safety SE209 element of the Technologies for Airplane State Awareness project, a sub-project in the NASA Airspace Operations and Safety Program.

References

[1] Cunningham, K., Shah, G. H., Frink, N. T., McMillin, S. N., Murphy, P. C., Brown, F. R., Shweyk, K. M., Nayani, S. N., "Preliminary Test Results for Stability and Control Characteristics of a Generic T-Tail Transport Airplane at High Angle of Attack," AIAA Atmospheric Flight Mechanics Conference, AIAA 2018-0529.

[2] Hyde, D. C., Brown, F. R., Shweyk, K. M., Cunningham, K., Shah, G., "High Angle of Attack Static and Dynamic Modeling Methods for Flight Dynamics Loss of Control," AIAA Atmospheric Flight Mechanics Conference, AIAA 2018-1021.

[3] Cunningham, K., Murphy, P. C., Shah, G. H., Frink, N. T., McMillin, S. N., , "Simulator Modeling for Stall Training," (to be published), AIAA SciTech Forum, January, 2019.

[4] Murphy, Patrick C. and Klein, Vladislav, "Validation of Methodology for Estimating Aircraft Unsteady Aerodynamic Parameters From Dynamic Wind Tunnel Tests," AIAA Atmospheric Flight Mechanics Conference, AIAA 2003–5397, 2003.

[5] Murphy, Patrick C., Klein, Vladislav, Frink, Neal T.: Nonlinear Unsteady Aerodynamic Modeling Using Wind Tunnel and Computational Data. Journal of Aircraft. Vol. 54: 659-683, No. 2, March-April 2017. DOI: 10.2514/1.C033881.

[6] Murphy, Patrick C., Klein, Vladislav, and Frink, Neal T., "Unsteady Aerodynamic Modeling in Roll for the NASA Generic Transport Model," AIAA Atmospheric Flight Mechanics Conference, AIAA 2012-4652.

[7] Murphy, P.C., Frink, Neal T., S. Naomi McMillin, Cunningham, Kevin, Shah, Gautam H., "Efficient Unsteady Model Estimation Using Computational and Experimental Data," AIAA Atmospheric Flight Mechanics Conference, AIAA 2018-3622, June 2018.

[8] S. Naomi Millin, Frink, Neal T., Murphy, Patrick C., Cunningham, K., Shah, Gautam H., "Computational Study of a Generic T-tail Transport," (to be published), AIAA SciTech Forum, January, 2019.

[9] Frink, Neal T., Hiller, Brett R., Murphy, Patrick C., Cunningham, Kevin, Shah, Gautam H., "Investigation of Reduced-Order Modeling for Aircraft Stability and Control Prediction," (to be published), AIAA SciTech Forum, January, 2019.

[10] Frink, N. T., "Tetrahedral Unstructured Navier-Stokes Method for Turbulent Flows," AIAA Journal, Vol. 36, No. 11, November 1998, pp. 1975-1982.
[11] Frink, N. T., Pirzadeh, S. Z., Parikh , P. C., Pandya, M. J.(2000) "The NASA Tetrahedral Unstructured Software System". Aeronautical Journal, Vol. 104, No. 1040 (491-499). TetrUSS website: http://tetruss.larc.nasa.gov.
[12] Thompson, J.R., Frink, N.T., and Murphy, P. C., "Guidelines for Computing Longitudinal Dynamic Characteristics of a Subsonic Transport", AIAA Applied Aerodynamics Conference, AIAA 2010-4819, June 2010.
[13] Klein, Vladislav and Murphy, Patrick C., "Estimation of Aircraft Nonlinear Unsteady Parameters From Wind Tunnel Data," NASA TM-1998-208969, December, 1998.
[14] Klein, Vladislav and Morelli, Eugene, "Aircraft System Identification: Theory and Practice," 1st edition, AIAA Inc., Reston, Virginia, 2006.
[15] Morelli, E., "System IDentification Programs for AirCraft (SIDPAC)," http://software.nasa.gov, Accessed: 2018-05-16.
[16] Bommanahal, M. and Goman, M., "Nonlinear Unsteady Aerodynamic Modeling by Volterra Variational Approach," AIAA Atmospheric Flight Mechanics Conference, AIAA 2012-4654.
[17] Pandya, M. J., Jespersen, D. C., Diskin, B., and Thomas, J. L., "Accuracy, Scalability and Efficiency of Mixed-Element USM3D for Benchmark Three-Dimensional Flows," (to be published), AIAA SciTech Forum, January, 2019.

Figures

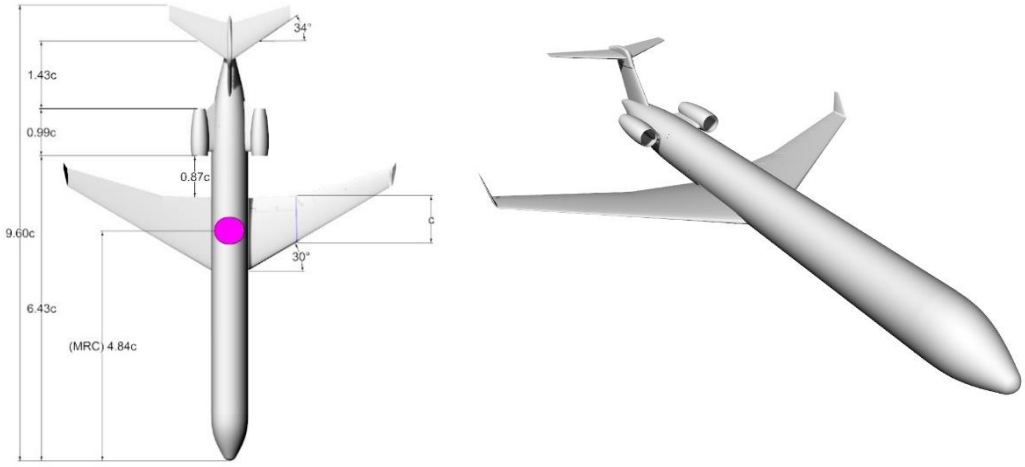

S = 40.90 in^2, $\bar{c}$ = 02.58 in, b = 17.78 in

Figure 1. GTT model geometry and perspective view.

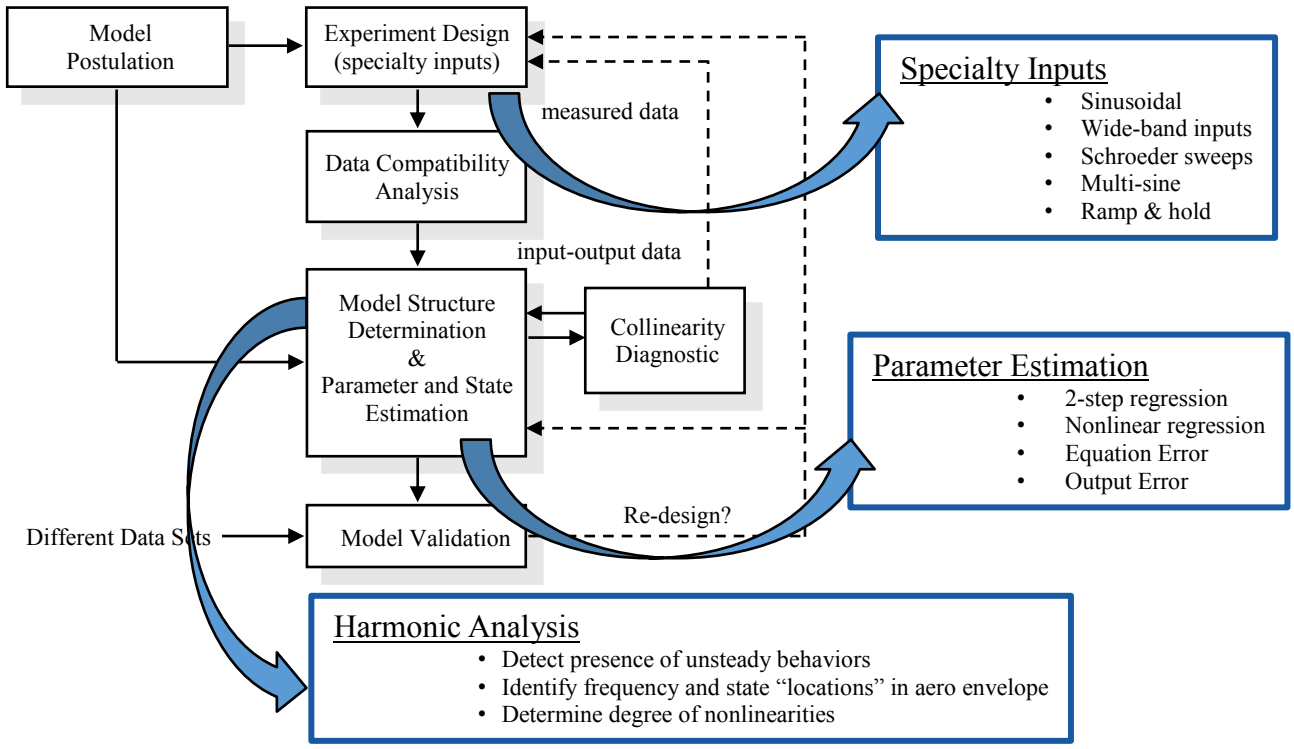

Figure 2 Aircraft System Identification for unsteady modeling.

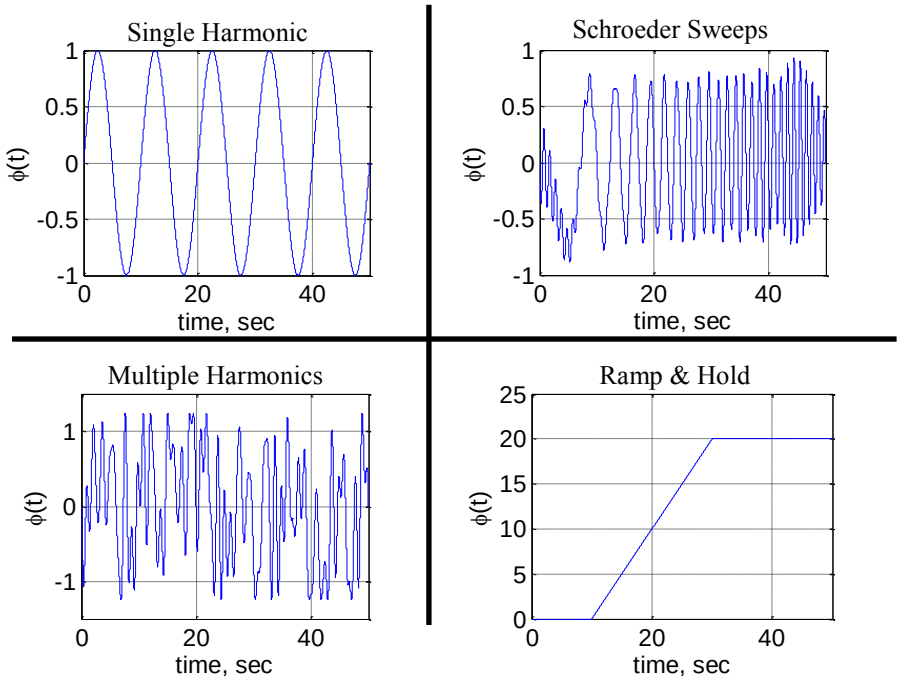

Figure 3. Conventional inputs for identification of unsteady models.

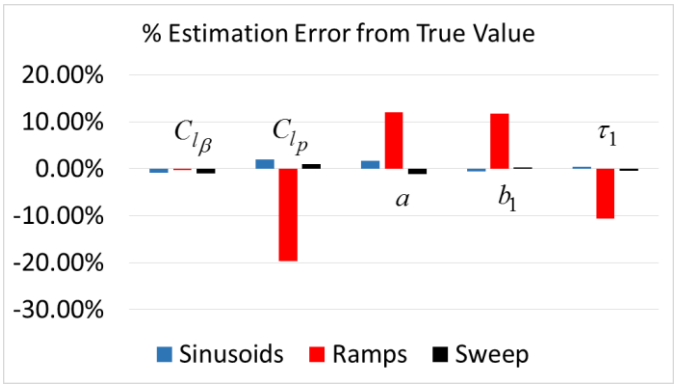

Figure 4. Modeling errors using three candidate inputs (Ref. 7).

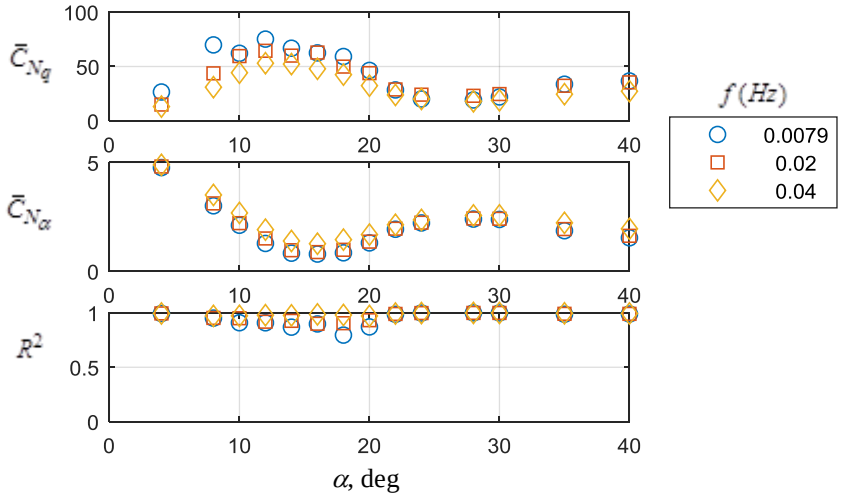

Figure 5a. Harmonic analysis of C_N using first-order model and data from CFD forced oscillations in pitch for three frequencies, α_A=5°, GTT model.

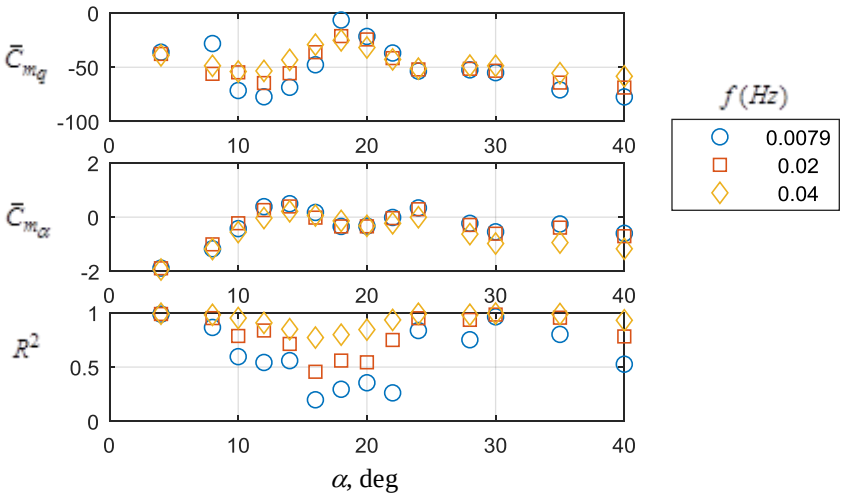

Figure 5b. Harmonic analysis of C_m using first-order model and data from CFD forced oscillations in pitch for three frequencies, α_A=5°, GTT model.

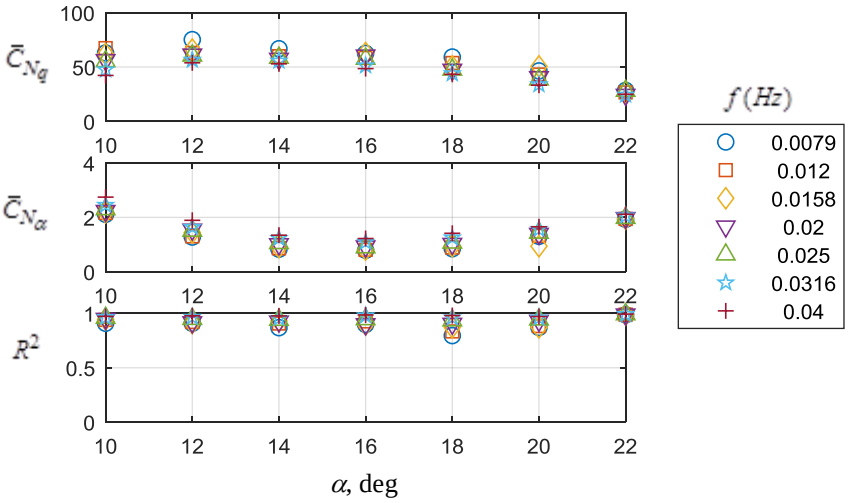

Figure 6a. Harmonic analysis of C_N using first-order model and data from CFD forced oscillations in pitch for seven frequencies, α_A=5°, GTT model.

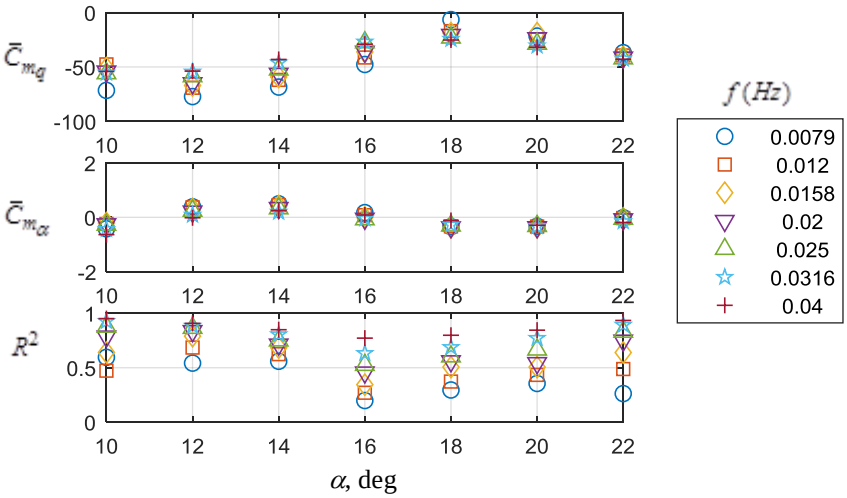

Figure 6b. Harmonic analysis of C_m using first-order model and data from CFD forced oscillations in pitch for seven frequencies, α_A=5°, GTT model.

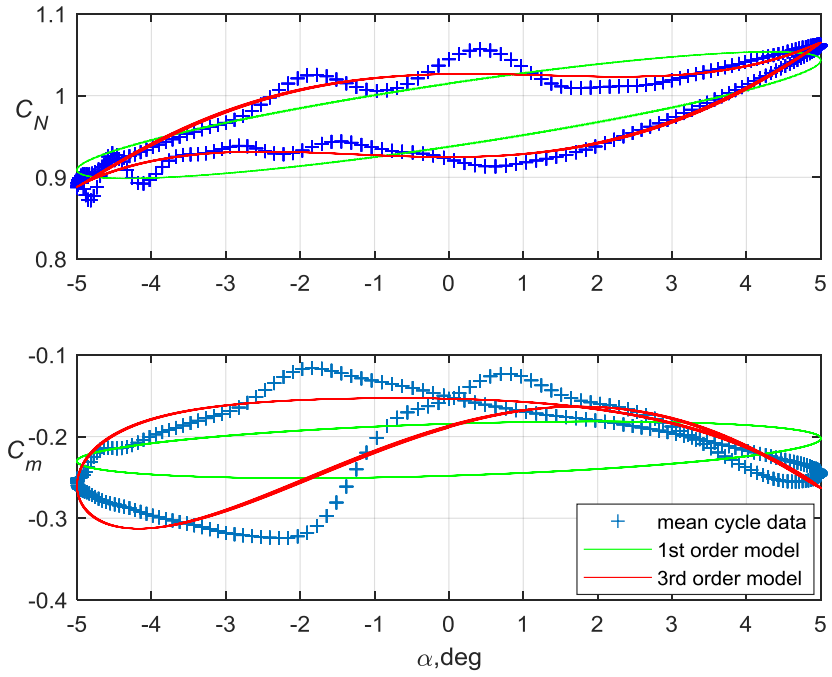

Figure 7. First and Third-order harmonic model and CFD simulated measurements for C_N and C_m at k = 0.0079, GTT model.

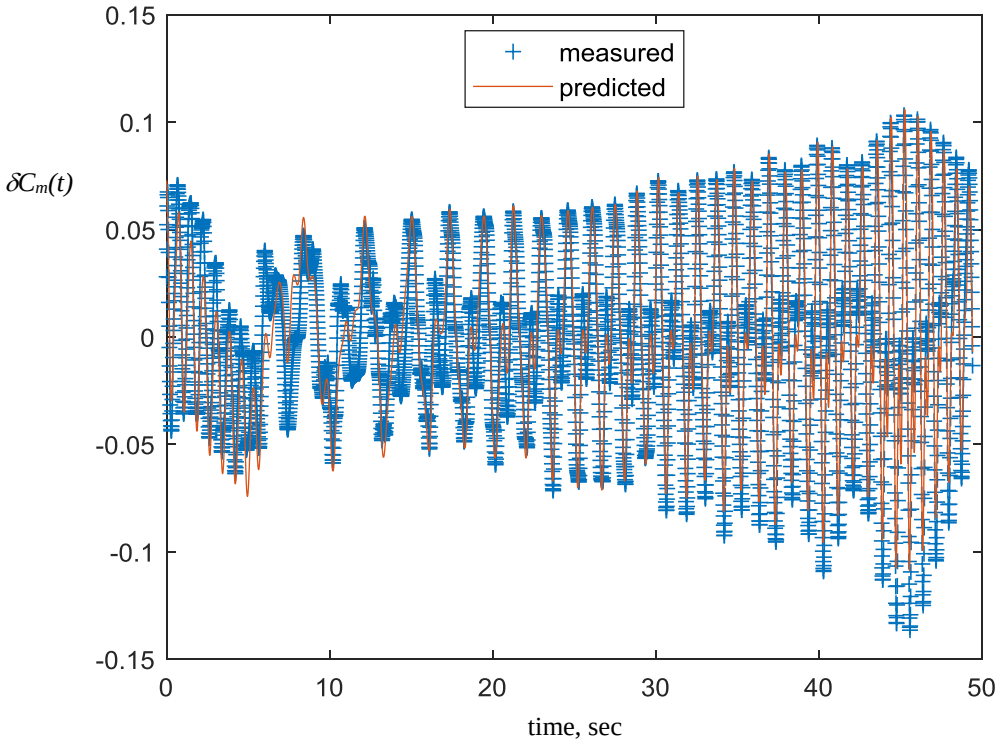

Figure 8. CFD simulated Schroeder sweep measurements and nonlinear unsteady model prediction C_m at α_0 = 16°, GTT model.

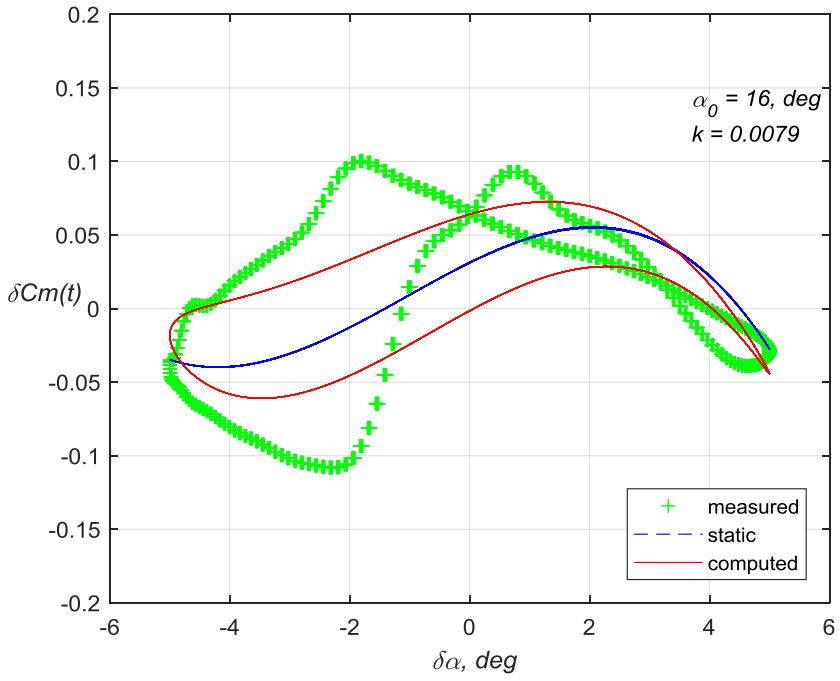

Figure 9. Third-order unsteady model and CFD "measurements" for C_m at k = 0.0079, GTT model, sinusoidal inputs.

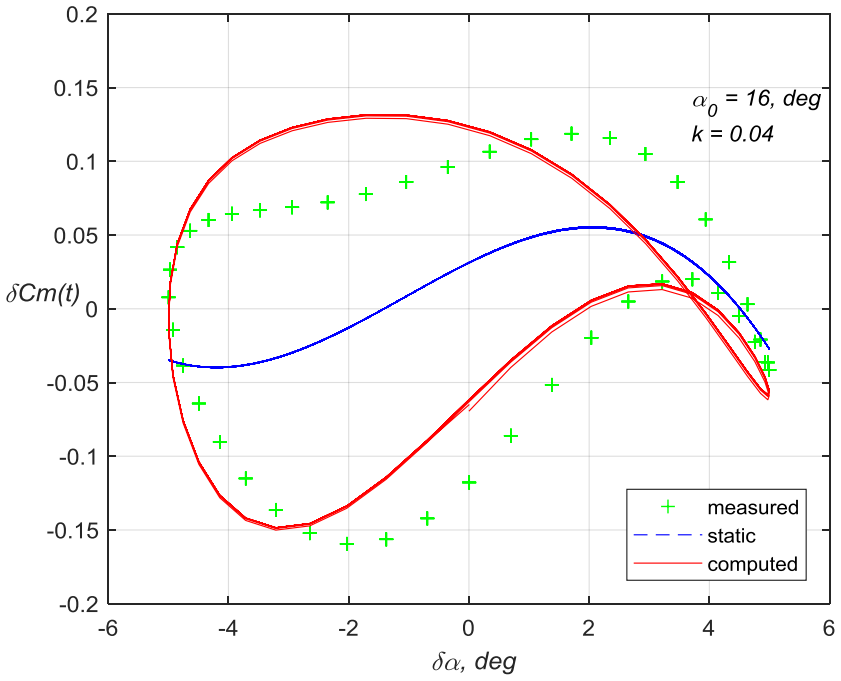

Figure 10. Third-order unsteady model and CFD "measurements" for C_m at k = 0.0400, GTT model, sinusoidal inputs.

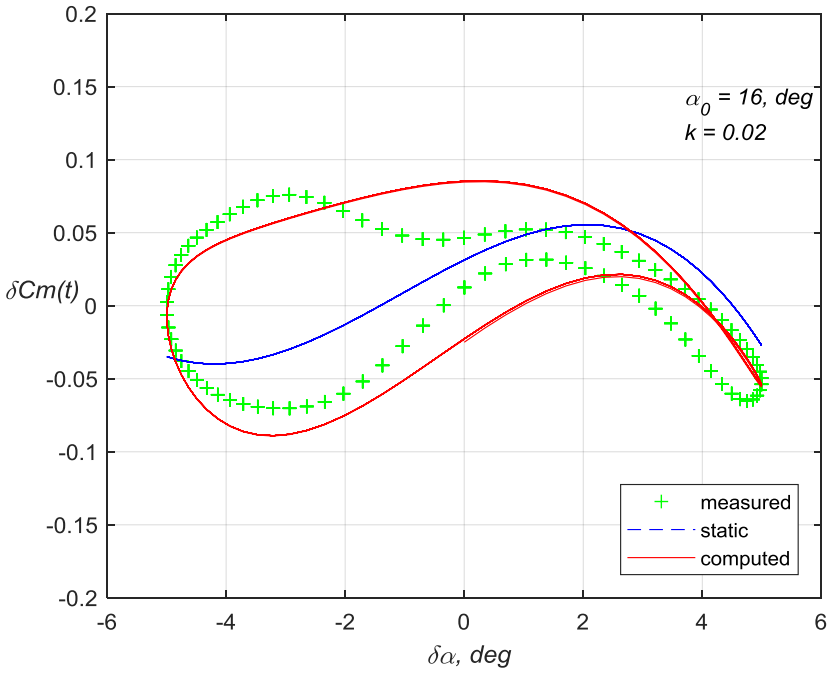

Figure 11. Validation Test. Third-order unsteady model and CFD "measurements" for C_m at k = 0.0200, GTT model, sinusoidal inputs.

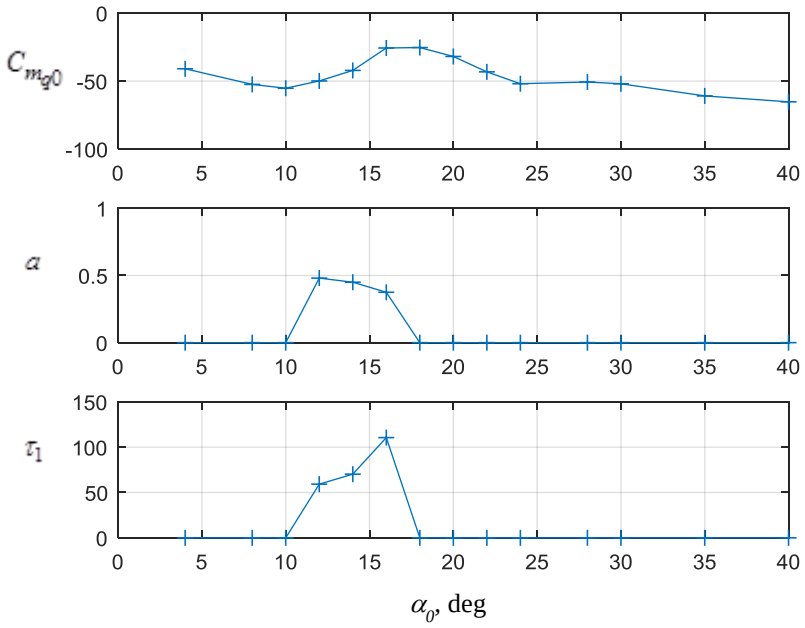

Figure 12. Primary dynamic model terms for C_m over the full range of angle of attack, based on CFD simulated responses to sinusoidal inputs.